

UC Berkeley

UC Berkeley Previously Published Works

Title

The impulsive effects of momentum transfer on the dynamics of a novel ocean wave energy converter

Permalink

<https://escholarship.org/uc/item/84w190kg>

Journal

Journal of Sound and Vibration, 332(21)

ISSN

0022-460X

Authors

Diamond, Christopher A
O'Reilly, Oliver M
Savaş, Ömer

Publication Date

2013-10-01

DOI

10.1016/j.jsv.2013.05.030

Peer reviewed

The impulsive effects of momentum transfer on the dynamics of a novel ocean wave energy converter

Christopher A. Diamond^a, Oliver M. O'Reilly^{a,*}, Ömer Savaş^a

^a*Department of Mechanical Engineering, University of California at Berkeley, Berkeley CA 94720, USA*

Abstract

In a recent paper by Orazov et al. (“On the dynamics of a novel ocean wave energy converter,” *Journal of Sound and Vibration* 329 (24) (2010) 5058–5069), a wave energy converter (WEC) was proposed. The converter features a mass modulation scheme and a simple model was used to examine its efficacy. Unfortunately, the simple model did not adequately account for the momentum transfer which takes place during the mass modulation. The purpose of the present paper is to account for this transfer and to show that the WEC equipped with a novel and more general mass modulation scheme has the potential to improve its energy harvesting capabilities.

Keywords:

Wave Energy Converter, Energy Harvesting, Resonance, Hybrid System

1. Introduction

In a recent paper [1] a novel wave energy converter (WEC) was proposed. The WEC featured a mass modulation scheme to improve the traditional energy harvesting capabilities of the WEC which employed resonant tuning.

*Corresponding author, Tel.: +1 510 642 0877, oreilly@berkeley.edu

Subsequent works [1, 2, 3, 4] on the mass modulated energy harvester analyzed the dynamics of a simple model for the WEC and implemented and tested the mass modulation scheme in a prototype device. After reviewing the experimental results in [3], it became apparent that the model presented in [1] and analyzed in [2, 4] was deficient. The deficiency was the failure to account for the impulse induced by the mass modulation system on the WEC.

The purpose of the current paper is to present a modified model for the mass modulated WEC, to comment on the changes to the results in [1] this modification produces, and to present a new mass modulation scheme which demonstrates the efficacy of a mass modulation scheme to improve the energy harvesting capabilities of a WEC.

2. A Generalized Model for a Mass Modulated WEC

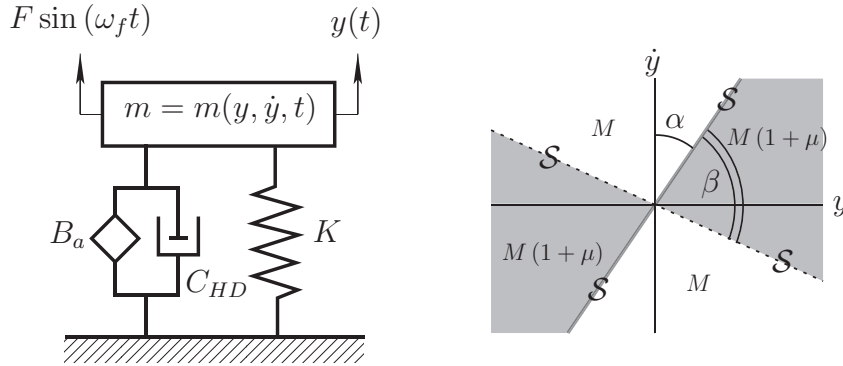


Figure 1: Schematic for a model for the mass modulated energy converter. The mass m of the oscillator depends on the sign of y and \dot{y} : $m = M(1 + \mu)$ or $m = M$. The most general case is shown; the rays \mathcal{S} correspond to the locations in the state space where water is either trapped or released.

Previous work laid out motivation for the basis of our model; it has been known that parametric excitation through time variance of key parameters can produce mechanical amplification in the response of a resonator. Subsequently, a model was created to represent a WEC that incorporated an added mass effect twice within each cycle; this sort of parametric variance indicates a hybrid dynamical system, which are known to have unexpected complexity (which we expected to increase harvested power) and a tendency toward instability (which was to be avoided). More in-depth background may be seen in [1, 2, 3] for the interested reader.

Departing from what was considered previously, we endeavored to create a general mathematical model for the conditions upon which the system's mass is modulated. By varying parameters in this model, we could determine the optimal regions (in phase space) to 'add' mass and then analyze this 'optimal' case numerically. As shown in Figure 1, the revised model can be considered as a simple mass-spring-dashpot system equipped with a state-dependent mass. Following the dictates laid out in the introduction, switching conditions were devised that are visualized in Figure 1. Between angle α in the phase plane (defined off of the positive y -axis) and angle β (defined off of the ray created by α , called \mathcal{S}) the mass of the system is equal to $(1 + \mu)M$; this is repeated between $\alpha + \pi$ and $\beta + \pi$. In all other regions, the mass is equal to M . If we define a coordinate θ for the state space,

$$\theta = \arctan\left(\frac{y}{\dot{y}}\right) \text{ where } 0 \leq \theta < 2\pi, \quad (1)$$

then the equation of motion for the model features a set of differential equa-

tions

$$\left. \begin{aligned} (1 + \mu) M\dot{y} + C\dot{y} + Ky &= F \sin(\omega_f t), & \alpha < \theta < \alpha + \beta \text{ or } \alpha < \theta - \pi < \alpha + \beta \\ M\ddot{y} + C\dot{y} + Ky &= F \sin(\omega_f t), & \text{otherwise.} \end{aligned} \right\} \quad (2)$$

In (2), K is the stiffness coefficient, C is the overall damping coefficient (composed of the sum of the hydrodynamic damping C_{HD} and applied power take-off damping B_a), M is the mass, μ is the mass modulation parameter, and the superposed dot denotes the time derivative: $\dot{y} = \frac{dy}{dt}$. The pair of differential equations in (2) are coupled by a switching condition at the switching boundary \mathcal{S} which models the momentum transfer due to the change in mass. Generally, the change in momentum at a switching boundary is equivalent to an impulse on the system at that point, or

$$M^+ \dot{y}^+ - M^- \dot{y}^- = f.$$

Here, \dot{y}^- is the velocity just before the phase flow $(y(t), \dot{y}(t))$ pierces the switching boundary \mathcal{S} , \dot{y}^+ is the velocity at the instant when the phase flow exits the switching boundary \mathcal{S} , with M^+ and M^- defined similarly. As f is the result of fluid/body interactions that are difficult to characterize analytically, we approximate f as some portion of the pre-boundary momentum:

$$f = -(1 - \epsilon) M^- \dot{y}^-.$$

It follows that

$$M^+ \dot{y}^+ = \epsilon M^- \dot{y}^-,$$

where $(1 - \epsilon)$ is a (constant) coefficient indicating the amount of momentum loss across \mathcal{S} . By varying ϵ 's value, we may estimate the varying effect of

the impulse f without actually explicitly determining it. The precise value of ϵ for a particular WEC will reflect the efficiency of the water entrapment mechanism. In [1, 2, 4], the case $\epsilon = (1 + \mu)$ was exclusively considered. This prescription for ϵ can be questioned on physical grounds because it implies that a positive impulsive force is needed to achieve the mass modulation: this force is absent from physical realizations of the WEC; so we then expect that without external momentum impulse $\epsilon \leq 1$. Such a prescription makes sense intuitively, as one would not expect an increase in momentum across any switching boundary without external forcing. With this in mind, we may consider two cases for the switching condition. The first pertains to when fluid is trapped (and mass is effectively added):

$$(1 + \mu) M \dot{y}^+ = \epsilon M \dot{y}^-. \quad (3)$$

When fluid is released (and mass is effectively removed), the switching condition is

$$M \dot{y}^+ = \epsilon (1 + \mu) M \dot{y}^-. \quad (4)$$

This condition pertains to the case when the phase flow passes through the switching boundary \mathcal{S} and the mass changes from $(1 + \mu)M$ to M .

The system (2)-(4) is known as a hybrid dynamical system and exhibits dynamics which are distinct from those found in single degree-of-freedom models for WECs and other energy harvesting devices that are discussed in, for example, [5, 6]. We note that when the stiffness K , damping C and mass M coefficients for this model are prescribed for a prototype WEC design, they will contain contributions from hydrostatic and structural elements. In addition, the parameter μ should not be confused with the added mass due

to hydrodynamic effects. The latter mass is crudely lumped into the mass parameter M in the simple model.

In our discussion of the dynamics of (2)-(3), we will use the dimensionless parameters δ and ω , dimensionless force amplitude f , and a dimensionless time τ :

$$\delta = \frac{C}{2\sqrt{KM}}, \quad \omega = \left(\sqrt{\frac{M}{K}}\right) \omega_f, \quad f = \frac{F}{K\ell}, \quad \tau = \left(\sqrt{\frac{K}{M}}\right) t. \quad (5)$$

Here, ℓ is a length scale.

3. Stability in the Unforced System

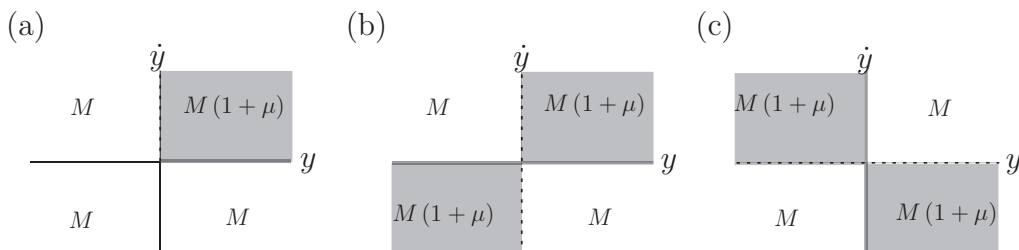


Figure 2: Three examples of mass modulation schemes denoted respectively as (a), Scheme I, (b) Scheme II, and (c) Scheme III. Scheme I is featured in the experimental work in [3], Scheme II is the case considered in [1, 2, 4], and Scheme III is an optimal energy harvesting scheme.

A feature of the hybrid dynamical system (2)-(4) or, moreover, any hybrid dynamical system, is the potential for oscillations $y(t)$ to become unbounded even in the absence of forcing ($F = 0$); in such a system the unforced system's stability is indicative of the forced system's stability—hence our interest in the $F = 0$ case. To examine this behavior we follow the arguments used in [1] to

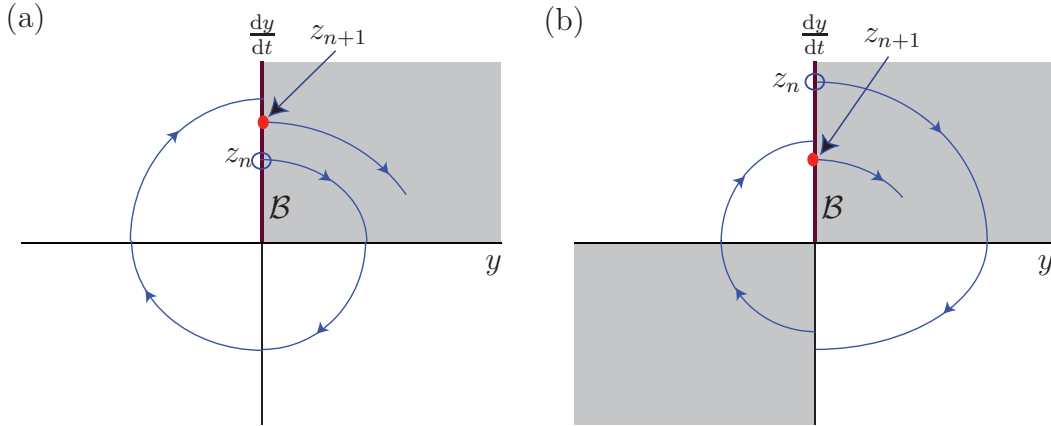


Figure 3: Schematic of the phase flows for the pair of hybrid systems corresponding to (a) Scheme I and (b) Scheme II. In both figures, the set \mathcal{B} denotes the positive y axis, the point z_n labeled with a disk is the starting point for the orbit and the solid disk is the point z_{n+1} where this trajectory first returns to intersect \mathcal{B} . In (a) a hypothetical case where the origin is unstable is shown, while the origin in (b) would be classified as stable.

examine the stability of the origin of the unforced hybrid system. Referring to Figure 2, three distinct mass modulation schemes are considered. In the first, which we refer to as Scheme I, there is only one instance of mass entrapment and release and in the second, which we refer to as Scheme II, there are two such instances. The system discussed so far in the literature correspond to the Scheme II with the questionable condition $\epsilon = 1 + \mu$. The third case, Scheme III, corresponds to a case where the energy harvesting was found to be optimal, as explained in Section 4.

The boundedness of solutions to (2)-(4) with $F = 0$ can be readily assessed using a Poincaré map. Referring the reader to Figure 3, an initial condition $(0, y_0)$ starting on the positive y axis is considered. Then, by using the piecewise exact solutions for the unforced system, the behavior of the

trajectory $(y(t), \dot{y}(t))$ can be determined. After a given period of time, the trajectory traverses the positive \dot{y} axis and the evolved value of \dot{y}_0 can be recorded and the process is repeated. We denote the sequence of values of \dot{y} by the variable z_1, \dots, z_n, \dots with $z_1 = \dot{y}_0$ and define a Poincaré map:

$$z_n = pz_{n-1}, \quad n \in \mathbb{Z}^+. \quad (6)$$

If $|p| < 1$, then the Poincaré map is non-expansive and $z_n \rightarrow 0$ as $n \rightarrow \infty$. In this case, we can state that the solutions to the equations of motion for (2)-(4) with $F = 0$ remain bounded and the origin is stable.

3.1. Scheme I

For Scheme I, the Poincaré map can be expressed as

$$z_{n+1} = \left(\frac{\epsilon h}{1 + \mu} \right)^2 z_n, \quad (7)$$

where the function h is

$$h = h(\mu, \delta) = \frac{1}{\omega_{n_1}} e^{(-\delta T_2)} e^{(-\delta_1 T_1)}. \quad (8)$$

In (8), the times of flight T_1 and T_2 are the smallest strictly positive solutions of

$$\sin(\omega_{d_1} T_1) = \left(\frac{\omega_{d_1}}{\delta_1} \right) \cos(\omega_{d_1} T_1), \quad \sin(\omega_d T_2) = - \left(\frac{\omega_d}{\delta} \right) \cos(\omega_d T_2), \quad (9)$$

and the dimensionless damping parameter and frequencies featuring in (8) and (9) are

$$\delta_1 = \delta \omega_{n_1}^2, \quad \omega_n = 1, \quad \omega_{n_1} = \frac{1}{\sqrt{1 + \mu}}, \quad \omega_d = \sqrt{1 - \delta^2}, \quad \omega_{d_1} = \omega_{n_1} \sqrt{1 - \delta^2 \omega_{n_1}^2}. \quad (10)$$

These parameters feature prominently in the piecewise analytical solutions that can be obtained for the hybrid system.¹

3.2. Scheme II

For Scheme II, the Poincaré map can be expressed as

$$z_{n+1} = \left(\frac{\epsilon q}{1 + \mu} \right) z_n, \quad (11)$$

where the function q is

$$q = q(\mu, \delta) = \frac{1}{\omega_{n1}} e^{(-\delta T_3)} e^{(-2\delta T_2)} e^{(-\delta_1 T_1)} \quad (12)$$

In this equation, the time of flight T_3 is the smallest strictly positive solution of

$$\sin(\omega_d T_3) = \frac{\omega_d}{\delta} \cos(\omega_d T_3). \quad (13)$$

3.3. Scheme III

For Scheme III, the Poincaré map can be expressed as

$$z_{n+1} = (\epsilon k (1 + \mu))^2 z_n, \quad (14)$$

where the function k is

$$k = k(\mu, \delta) = \omega_{n1} e^{(-\delta_1 T_5)} e^{(-\delta T_4)}. \quad (15)$$

In (15), the times of flight T_4 and T_5 are the smallest strictly positive solutions of

$$\sin(\omega_d T_4) = \left(\frac{\omega_d}{\delta} \right) \cos(\omega_d T_4), \quad \sin(\omega_{d1} T_5) = - \left(\frac{\omega_{d1}}{\delta_1} \right) \cos(\omega_{d1} T_5). \quad (16)$$

¹The expression (10)₅ for ω_{d1} corrects a typographical error in the expression for this frequency that is present in [1, 2].

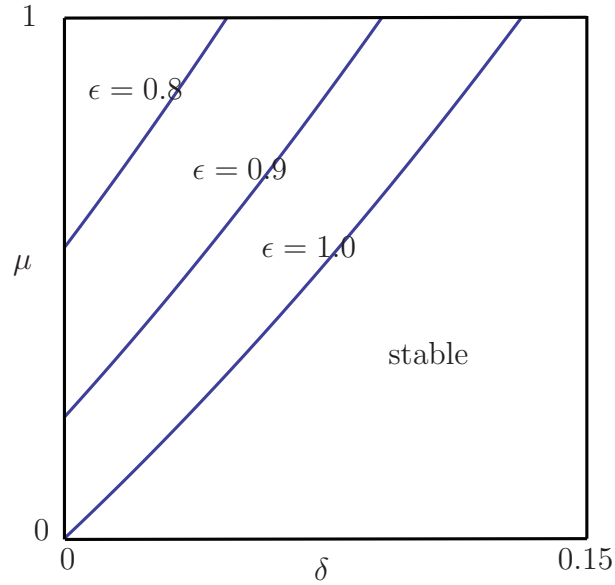


Figure 4: Stability boundaries in the $\delta - \mu$ plane for the unforced response of the hybrid system featuring Scheme III. As ϵ gets smaller, the stable region of the $\mu - \delta$ plane increases in size. For various values of ϵ , μ , and δ , the boundaries were obtained with the assistance of (19).

The dimensionless damping parameter and frequencies featuring in (15) and (16) are presented in (5) and (10).

3.4. Bounded and unbounded responses of the unforced system

We can now readily analyze the growth or decay of solutions to the unforced system. For the first two mass modulation schemes, we observe that the solutions will always remain bounded provided $\epsilon \leq 1$. To see this we observe from (7) and (11) that as $\mu \geq 0$,

$$q \leq \frac{1}{\omega_{n_1}} = \sqrt{1 + \mu}, \quad h^2 \leq \frac{1}{\omega_{n_1}^2} = 1 + \mu. \quad (17)$$

With the expressions for p featuring in the Poincaré maps, we note that

$$\frac{\epsilon}{1+\mu}q \leq \frac{\epsilon}{\sqrt{1+\mu}}, \quad \left(\frac{\epsilon}{1+\mu}\right)^2 h^2 \leq \frac{\epsilon}{1+\mu} \quad (18)$$

In conclusion, if $\epsilon \leq 1$, then the origin will never be unstable; fortuitously, this corresponds exactly to the physically realizable values for ϵ available to our system. This result is in contrast to our earlier works [1] where we erroneously assumed that $\epsilon = 1 + \mu$. It is interesting to note that the momentum transfer modeled by (3) has a stabilizing effect on the system.

In contrast to the above cases, the third mass modulation scheme, Scheme III, can promote the growth of unbounded unforced responses. To see how this can be the case, we observe from (11) that

$$p = (\epsilon k (1 + \mu))^2 = \epsilon^2 (1 + \mu) e^{(-2\delta_1 T_5)} e^{(-2\delta T_4)}. \quad (19)$$

Depending on the values of ϵ , μ and δ , p can be greater than 1 and unbounded solutions of the hybrid system become possible. The regions in the $\delta - \mu$ parameter space where $p > 1$ for various values of ϵ can be seen in Figure 4.

4. Efficacy of the Modulation Scheme

In order to buttress the assertion that Scheme III is optimal, we must choose a metric by which the efficacy of any scheme may be measured. Here, similar to our earlier work [1], we take the power generated by our WEC as proportional to the velocity across the damping element B_a – or that such an element models a simple power take-off. As such, the nondimensional average power that can be harnessed from the oscillator (2)-(3) is defined as

$$P_{\text{av}} = \frac{B_a}{2T\sqrt{KM}} \int_0^T \left(\frac{du}{d\tau}\right)^2 d\tau, \quad (20)$$

where $u = y/\ell$ is the dimensionless vertical displacement of the system and T is a period of integration which is much larger than $2\pi/\omega$.

Ignoring, for the moment, the stability analyses of Section 3 we look at (3). This relation reveals that even with the 'best-case' value for parameter ϵ , i.e. $\epsilon = 1$ (which would correspond to no boundary momentum loss), any non-zero value of pre-boundary velocity \dot{y}^- and added mass μ would result in a post-boundary velocity \dot{y}^+ such that $|\dot{y}^+| < |\dot{y}^-|$; plainly, that adding mass, in tandem with the conservation of momentum, will reduce velocity. Similarly, it can be seen that the mass releasing boundary (4) will have the opposite characteristic—a velocity 'jump' corresponding to the release of mass. Intuitively, then, it makes sense that at the boundary associated with (3) we desire zero velocity and thus no momentum loss; at (4) we desire the maximum absolute velocity to profit most from the momentum 'jump' when mass is released. These desires correspond to choices of $\alpha = \frac{\pi}{2}$ and $\beta = \frac{\pi}{2}$: numerical simulations of power harvested with variance of α and β , along with various other system parameters, confirm this is the optimal case. So $\alpha = \frac{\pi}{2}$ and $\beta = \frac{\pi}{2}$ is optimal (illustrated in Figure 2 (c)), and it is this case that will be considered.

Results for the numerical simulation of (2)-(3), specifically in the case of Scheme III, are shown in Figures 5 and plots of average harnessed power P_{av} for several combinations of added mass μ and damping δ are shown in Figure 6. The prominent feature of the phase diagram in Figure 5 is the jump in velocity at the moment of mass entrapment (i.e., at the switching boundary $\dot{y} > 0$ and $y = 0$). The simulations show that the simplified excitation scheme, while not as effective as the originally proposed version, is still able

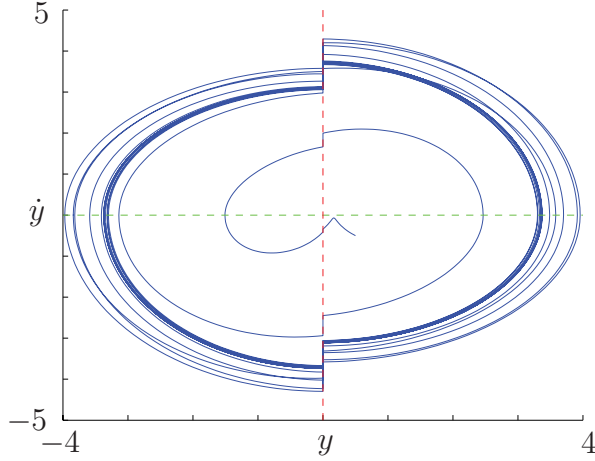


Figure 5: Phase portrait of system configured to Scheme III ($\alpha = \frac{\pi}{2}$, $\beta = \frac{\pi}{2}$), with $\omega = 1$, $\delta = 0.08$, $\mu = 0.5$, $f = 1$, and $\epsilon = 0.8$. Notice the velocity jump attributable to the switching conditions (3)-(4) along the red dotted line.

to generate an increase in oscillation amplitude and improve the harnessed power (see Figure 6) over a non-mass modulated buoy WEC.

5. Conclusions

It may be noted that due to the model being directly excited by a wave induced force $f(t)$, instead of seismically excited by an incident wave of amplitude $A(t)$, its efficiency may not be directly compared to results from [5, 7, 8]: methods in said papers would necessitate the ability to specify both a WEC volume V and incoming wave amplitude A . Our scheme does not require a specific geometry but rather assumes that the mass modulation may be accomplished in varied geometries through different means; once a desired geometry is specified, a frequency transfer function may be produced

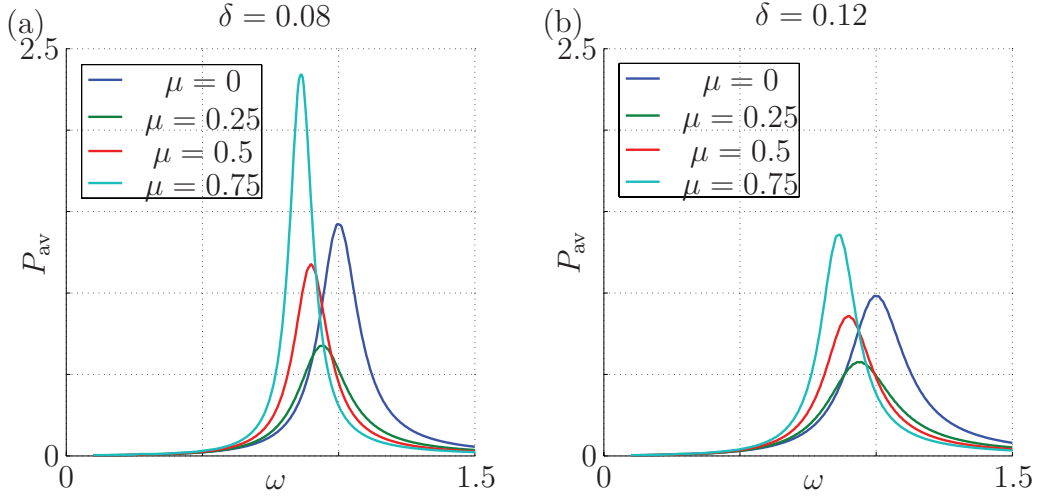


Figure 6: Average nondimensional power P_{av} for Scheme III ($\alpha = \frac{\pi}{2}, \beta = \frac{\pi}{2}$), as in Figure 2 (c), as a function of driving frequency ω for various values of μ and δ . Selected values of damping parameter δ are indicated on the figure and the switching boundary momentum loss $\epsilon = 0.8$. For these simulations, $\sqrt{K/M} = 1$ and the non-dimensional forcing $f = 1$. In (a) $\delta = 0.08$ and in (b) $\delta = 0.12$.

allowing for the relation between the force $f(t)$ in the model and incoming wave amplitude A . In other words, the simplicity and flexibility of the scheme which allow for its adaptation in many situations effectively disallows a direct comparison with existing metrics.

It is still desirable to compute the efficiency of the scheme in terms of the power applied by the wave force $f(t)$. As the input wave amplitude is not known, it suffices to use the simple assumption that the power of the force is $P_{\text{in}} = f(t) \cdot \frac{dy}{dt}$, noting that as the mass modulation scheme changes the dynamics of the system, P_{in} will change for different choices of μ . As can be seen from Figures 6 and 7, added mass lowers the resonant frequency

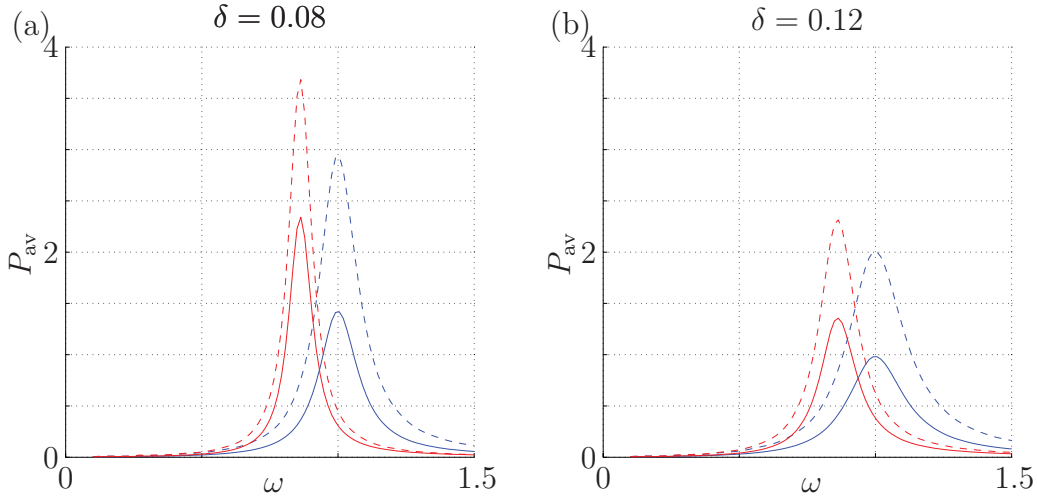


Figure 7: Comparison of average nondimensional power applied to the model P_{in} (dotted lines) and average nondimensional power collected P_{av} (solid lines) for same selections of parameters as in Figure 6; the blue lines correspond to $\mu = 0$ and the red lines to $\mu = 0.75$. (a) Recovers 64.64% of the input power across the shown frequency range, with $\mu = 0.75$; with $\mu = 0$ it recovers 48.51%. (b) Recovers 59.31% with $\mu = 0.75$ and 49.03% with $\mu = 0$.

of the system and increases (past a certain value of μ) the power that may be harvested compared to the non-modulated case (i.e, $\mu = 0$ and $\epsilon = 1$). Additionally, from Figure 7, the scheme changes the dynamics of the system such that the maximum available power is shifted lower in the frequency range and the power band is more narrow than the $\mu = 0$ case. However, within the confines of the power available to both schemes, the added mass case captures a higher percentage of that power than the $\mu = 0$ case.

As discussed in [3], experimental realizations of Scheme II turned out to be very difficult to achieve and this lead to the implementation of Scheme I in [3]. Unfortunately, this simpler mass modulation scheme was not very effective

in improving the energy harvesting capabilities of a WEC. The analysis of the new Scheme III that we have presented has the potential to produce the desired energy harvesting improvements. To this end, we are currently developing a more complex, two degree-of-freedom (DOF) model which more accurately models a WEC along with its fluid-structure interactions. In addition, efforts are underway to design an experimental implementation of Scheme III. The design of this mechanism will leverage our earlier designs that are discussed in [3].

Acknowledgements

This research was partially supported by grant number CMMI-1000906 from the U. S. National Science Foundation. The authors are also grateful to Dr. Bayram Orazov for his earlier work on the WEC and Prof. Carolyn Judge for her helpful comments on the implementation of the mass modulation system. Finally, the authors are grateful to the anonymous reviewer of an unpublished manuscript for their constructive comments on the impulsive loading caused the mass modulation system on the WEC.

References

- [1] B. Orazov, O. M. O'Reilly, Ö. Savaş, [On the dynamics of a novel ocean wave energy converter](#), Journal of Sound and Vibration 329 (24) (2010) 5058–5069.
URL <http://dx.doi.org/10.1016/j.jsv.2010.07.007>
- [2] B. Orazov, O. M. O'Reilly, X. Zhou, [On forced oscillations of a simple model for a novel wave energy converter: non-resonant instability, limit](#)

- cycles, and bounded oscillations, *Nonlinear Dynamics* 67 (2) (2012) 1135–1146.
URL <http://dx.doi.org/10.1007/s11071-011-0058-7>
- [3] B. Orazov, A novel excitation scheme for an ocean wave energy converter, Ph.D. thesis, University of California at Berkeley (2011).
- [4] A. Rougirel, [Mathematical analysis of a wave energy converter model](#), *Nonlinear Analysis: Real World Applications* 14 (1) (2013) 434–454.
URL <http://dx.doi.org/10.1016/j.nonrwa.2012.07.007>
- [5] J. Falnes, [Wave energy conversion through relative motion between two single-mode oscillating bodies](#), *Journal of Offshore Mechanics and Arctic Engineering* 121 (1) (1999) 32–39.
URL <http://dx.doi.org/10.1115/1.2829552>
- [6] N. G. Stephen, [On energy harvesting from ambient vibration](#), *Journal of Sound and Vibration* 293 (1–2) (2006) 409–425.
URL <http://dx.doi.org/10.1016/j.jsv.2005.10.003>
- [7] J. Falnes, [A review of wave-energy extraction](#), *Marine Structures* 20 (4) (2007) 185–201.
URL <http://dx.doi.org/10.1016/j.marstruc.2007.09.001>
- [8] J. Falnes, J. Hals, [Heaving buoys, point absorbers and arrays](#), *Philosophical Transactions of the Royal Society A: Mathematical, Physical and Engineering Sciences* 370 (1959) (2012) 246–277.
URL <http://dx.doi.org/10.1098/rsta.2011.0249>